Topological degree theory and local analysis of area preserving maps

C. Polymilis
Department of Physics, Athens University, Panepistimiopolis, GR-15784 Zografos, Athens, Greece

G. Servizi
Department of Physics, Bologna University, Via Irnerio 46, I-40126 Bologna, Italy
and I.N.F.N. Sezione di Bologna, Via Irnerio 46, I-40126 Bologna, Italy

Ch. Skokos
Department of Mathematics, Division of Applied Analysis and Center of Research and Applications
of Nonlinear Systems (CRANS), University of Patras, GR-26500 Patras, Greece
and Research Center for Astronomy, Academy of Athens, Anagnostopoulou 14, GR-10673 Athens, Greece

G. Turchetti
Department of Physics, Bologna University, Via Irnerio 46, I-40126 Bologna, Italy
and I.N.F.N. Sezione di Bologna, Via Irnerio 46, I-40126 Bologna, Italy

M. N. Vrahatis
Department of Mathematics, University of Patras, GR-26110 Patras, Greece
and University of Patras Artificial Intelligence Research Center (UPAIRC), University of Patras,
GR-26110 Patras, Greece

We consider methods based on the topological degree theory to compute periodic orbits of area preserving maps. Numerical approximations to the Kronecker integral give the number of fixed points of the map provided that the integration step is ''small enough.'' Since in any neighborhood of a fixed point the map gets four different combinations of its algebraic signs we use points on a lattice to detect the candidate fixed points by selecting boxes whose corners show all combinations of signs. This method and the Kronecker integral can be applied to bounded continuous maps such as the beam–beam map. On the other hand, they cannot be applied to maps defined on the torus, such as the standard map which has discontinuity curves propagating by iteration. Although the use of the characteristic bisection method is, in some cases, unable to detect all fixed points up to a given order, their distribution gives us a clear picture of the dynamics of the map. © *2003 American Institute of Physics.* [DOI: 10.1063/1.1539011]

In this paper we discuss the problem of localization of periodic orbits in two-dimensional mappings. We present numerical methods for computing the total number of periodic orbits of given period in bounded regions of the phase space and for locating their position. All these methods are based on the topological degree theory and their advantages are discussed in detail. The effectiveness of the characteristic bisection method, for locating high order periodic orbits is shown by applying it to different mappings on a plane and on a torus. For these mappings periodic orbits of order up to 40 were computed.

I. INTRODUCTION

Two-dimensional (2D) mappings are used to model dynamical systems with two degrees of freedom, conservative or dissipative depending on their *area-preserving* or *area-contracting* character. Their dynamical properties critically depend on the distribution and the nature of *periodic orbits*. Any point of a periodic orbit of period p is a *fixed point* of the map M iterated p times ($M^{\circ p}$). A fixed point of $M^{\circ p}$ is sometimes called fixed point of M of order p. The fixed points of area preserving maps are classified as *elliptic, parabolic, hyperbolic* and *hyperbolic with reflection*, according to how the eigenvalues of the Jacobian matrix are laid out on the complex plane. In particular the fixed point is stable when the corresponding eigenvalues lie on the unit circle, hyperbolic when the eigenvalues have positive real values, hyperbolic with reflection when the eigenvalues have negative real values and parabolic when they are both 1 or −1: from a numerical point of view we decided to label as *parabolic* those fixed points which give Jacobian's eigenvalues very close to either 1 or −1 (by less than a predefined tolerance we fixed as 10^{-6}). The different stability types of fixed points in maps, as well as the possible transitions between these types, have been studied in detail in Refs. 1 and 2.

The possibility of finding the fixed points up to a given period is dynamically relevant and computationally challenging. Various methods exist to localize a periodic orbit once the region where it is located is known with a good accuracy, such as Newton's method and related classes of algorithms.[3,4] However, the determination of all or almost all the periodic orbits up to a given period is a long and often impossible task. Analytic expressions for the periodic orbits are known only for very low periods and efficient numerical methods are available only if the map can be decomposed into involutions. For the Hénon map the fixed points up to period 4 were found analytically[5] and for the standard map the involution method allowed the detection of periodic orbits of very long periods approaching the golden invariant curve.[6]

The traditional iterative schemes with quadratic convergence such as Newton's method and related classes of algorithms are frequently used. These methods converge rapidly for any initial guess in a region where a single fixed point is present. This is rarely the case since the fixed points form a dense set. Moreover if the order p is not a prime number, i.e., p is of the form $p = p_1^{k_1} \cdots p_m^{k_m}$, the search of the fixed points of order p provides also all the fixed points of order $p_1, \ldots, p_m$. This problem could be solved using deflation methods, but their exponential growth with p entails serious difficulties. These methods are affected by errors due to the large values the map can assume in a neighborhood of hyperbolic points or due to poor regularity of the partial derivatives.

As an alternative the use of methods based on the application of *topological degree* (TD) theory has been proposed.[7] Degree theory[8] and its application to solve systems of nonlinear equations[3,4] has been extensively considered in the mathematical literature starting from the works of Kronecker,[9] Picard,[10,11] and Hadamard[12] until recent times.[13–16] The TD gives a criterion to insure the existence of fixed points in a bounded domain and the Kronecker integral[9,12] allows to determine their number.[10,11] The actual localization can be reached using the *characteristic bisection method*.[7,17,18]

These methods prove to be efficient in localizing the fixed points of 2D and even 4D maps[7,19,20] once a good initial guess is given by direct inspection of the orbits as it is often the case with graphical interactive programs for maps of $\mathbb{R}^2$ (e.g., the program GIOTTO[21]). However the localization of all or at least a large fraction of the fixed points of a given order in a compact region requires well tailored strategies. The associated dynamical information is relevant because to know the location and nature of the fixed points amounts to knowing the properties of the mapping. Another possibility is to examine directly the bifurcations occurring when a parameter is varied.[22,23] An alternative is the discretization of the map replacing the original one with a permutation map on a lattice.[24]

In this paper, we propose to use the characteristic bisection method[7,17,18] to compute the periodic orbits up to a given order in a compact region. This method exploits TD theory to provide a criterion for the existence of fixed points. Starting from a box, where the TD is ± 1, and refining it, a fixed point is localized with the desired accuracy. This method has been also applied successfully to Hamiltonian systems of 2 degrees of freedom.[25–27] The detection of all fixed points of order p in a compact domain is a hard task as shown by a simple topological argument. Assigning to any point a color corresponding to the signs of the components of $M^{\circ p} - I$, where I is the identity, we obtain a *color-map*. A compact set is painted with four colors so, when four distinct colors appear in a region a simple fixed point exists at the intersection of their boundaries. To set up a numerical strategy we consider a lattice obtained by partitioning the unit square with cells of size $\epsilon = 2^{-n}$. Among all the boxes of side $m\epsilon$, consisting of m^2 adjacent cells, we select those which have lattice points of four distinct colors as candidates to possess a fixed point in their interior, retaining at the end only one for every set of overlapping boxes. By increasing m from 1 to n the number of candidate fixed points approaches a constant value and the right number of fixed points is recovered as $n \to \infty$. The Kronecker integral gives the exact number of fixed points in a given domain, but the numerical accuracy depends on the distribution of fixed points and their distance from the boundary. If a fixed point approaches the boundary the mesh size should be much smaller than such a distance. A special care has to be taken for maps defined on the torus since discontinuity curves appear while the theorems for the TD hold in any subset where the map $M^{\circ p}$ is continuous. Stenger's method for computing the TD in a domain[16,28] is affected by the presence of fixed points near the border of the domain in a similar way.

We have studied three area preserving maps: the beam–beam map (BM)[23,29] and the Hénon quadratic map (HM),[5,22] both defined on $\mathbb{R}^2$, and the standard map (SM)[30] defined on the torus $\mathbb{T}^2$; among these we made a deeper analysis of (BM) and (SM). In the first case, where the map is continuous (holomorphic) the *color map* shows no obvious relation between the shape of the four colors domains close to the fixed point and the geometry of nearby orbits. Indeed, linearizing $M^{\circ p}$ in a small neighborhood of the fixed point, the boundaries of the four colors domains are two straight lines and their angle does not exhibit a simple dependence on the angle between the stable and unstable manifolds or on the ratio between the island's semiaxis.

The possibility of small angles for chains of large islands shows that an automatic detection algorithm based on the evaluation of the signs of $M^{\circ p}$ on a grid followed by the characteristic bisection method can miss some fixed points. In the case of the standard map the discontinuity curves of M propagate when the map is iterated and limit the use of the Kronecker integral and the *color map* to domains not intersected by these lines. In this case the characteristic bisection method can be applied to the whole plane, but we have to check that the computed fixed points correspond to real periodic orbits of the system.

Even though the choice of a lattice to initialize the characteristic bisection method on the squares whose corners have different combination of signs (corresponding to different colors) does not detect all the fixed points no matter how small is the lattice spacing, the picture which emerges, especially for the standard map, is dynamically meaningful (the discontinuity curves do not affect the result). One of the key advantages of the characteristic bisection method is that the computable information it requires consists on the algebraic signs of the components of the mapping. Thus it is not affected neither by the mapping evaluations taking large values in neighborhoods of unstable periodic orbits nor by precision losses until the last significant digit. This means that the method requires the knowledge of *only* the sign of various quantities and not their exact values.

II. THE TOPOLOGICAL DEGREE

We first consider the problem of detecting the zeroes of a function $F = (f_1, f_2)$ of class $\mathcal{C}^2$ on the closure of a bounded domain $\mathcal{D} \subset \mathbb{R}^2$ we assume to be the square of side $2L$. The function is defined by

$$x' = f_1(x,y), \quad y' = f_2(x,y). \tag{1}$$

The search of the fixed points of order p of a map M amounts to searching the zeroes of $F = M^{\circ p} - I$, where I is the identity map. The curves $\mathcal{F}_1 = \{(x,y) \in \mathcal{D}: f_1(x,y) = 0\}$ and $\mathcal{F}_2 = \{(x,y) \in \mathcal{D}: f_2(x,y) = 0\}$ split an open set $\mathcal{D}$ into the open sets $\mathcal{D}_{1\pm}$ and $\mathcal{D}_{2\pm}$ where f_1 and f_2 have the quoted signs

$$\text{sign}\, f_1(x,y) = \pm 1 \quad \text{for } (x,y) \in \mathcal{D}_{1\pm},$$
$$\text{sign}\, f_2(x,y) = \pm 1 \quad \text{for } (x,y) \in \mathcal{D}_{2\pm}. \tag{2}$$

Consider the intersections

$$\mathcal{D}_{++} = \mathcal{D}_{1+} \cap \mathcal{D}_{2+}, \quad \mathcal{D}_{+-} = \mathcal{D}_{1+} \cap \mathcal{D}_{2-},$$
$$\mathcal{D}_{-+} = \mathcal{D}_{1-} \cap \mathcal{D}_{2+}, \quad \mathcal{D}_{--} = \mathcal{D}_{1-} \cap \mathcal{D}_{2-}, \tag{3}$$

where the function $F = (f_1, f_2)$ has a certain combination of signs for f_1 and f_2. The zero of F is the intersection of $\mathcal{F}_1$ and $\mathcal{F}_2$ which are the common boundaries of $\mathcal{D}_{1+}$ and $\mathcal{D}_{1-}$, $\mathcal{D}_{2+}$ and $\mathcal{D}_{2-}$, respectively.

Any neighborhood of a simple zero (whose determinant of the corresponding Jacobian matrix is different from zero) of F has a nonempty intersection with the four domains $\mathcal{D}_{1+}\mathcal{D}_{1-}\mathcal{D}_{2+}\mathcal{D}_{2-}$. Coloring each domain with a different color, four different colors are found in any neighborhood of the zero. The TD[8] is defined as the difference $\mathcal{T}(F,\mathcal{D}) = r_+ - r_-$ between the number r_+ of zeroes with $\det J_F > 0$ and r_- with $\det J_F < 0$ where $\det J_F$ is the determinant of the Jacobian matrix J_F of F, and is given by the Kronecker integral[9,12]

$$\mathcal{T}(F,\mathcal{D}) = \frac{1}{2\pi} \oint_{b(\mathcal{D})} \frac{f_1 \, df_2 - f_2 \, df_1}{f_1^2 + f_2^2} = r_+ - r_-, \tag{4}$$

where the integral is computed counterclockwise on the boundary $b(\mathcal{D})$ of the given region $\mathcal{D}$ which, in our case, is a closed path.

Another way to compute the TD is Stenger's method[16,28] which consists of finding the signs of f_1, f_2 on a fine grid on the boundary of $\mathcal{D}$ (see Appendix B).

A. Error estimate

The contour integral (4) can be evaluated numerically in order to obtain the TD. The accuracy depends on the distance ϵ of the closest zero from the boundary. The integration step δ cannot exceed ϵ to have an error of order ϵ at least. To illustrate this we consider a simple example choosing two linear functions $f_1 = x$, $f_2 = y - 1 + \epsilon$ and a domain $\mathcal{D}$ defined by $|x| \le 1$, $|y| \le 1$. From (4) we find

$$\mathcal{T}(F,\mathcal{D}) = \frac{1}{\pi}\left[\arctan\frac{1}{\epsilon} + \arctan\frac{1}{2-\epsilon} + \arctan(\epsilon) \right.$$
$$\left. + \arctan(2-\epsilon) \right]. \tag{5}$$

Recalling that $\arctan(x) + \arctan(x^{-1}) = \pi/2 \, \text{sign}(x)$ we have $\mathcal{T} = 1$ if $0 < \epsilon < 2$ and for $\epsilon \to 0^+$ and $\mathcal{T} = 0$ if $\epsilon < 0$ and for $\epsilon \to 0^-$. The first term within the brackets comes from the upper side of the integration path

$$I = \frac{1}{2\pi} \int_{-1}^{1} \frac{\epsilon}{x^2 + \epsilon^2} dx = \frac{1}{\pi} \arctan\frac{1}{\epsilon} \simeq \frac{1}{2} - \frac{\epsilon}{\pi}. \tag{6}$$

The integration step has to be chosen of order ϵ in order to keep the error constant when $\epsilon \to 0$. Indeed letting N_ϵ be the integer part of ϵ^{-1} the integral (6) is approximated by using the rectangle rule with $2N_\epsilon + 1$ points in the interval $[-1,1]$

$$I \simeq \frac{1}{2\pi} \sum_{k=-N_\epsilon}^{N_\epsilon} \frac{1}{1+k^2} \simeq \frac{1}{2\pi} \sum_{k=-\infty}^{+\infty} \frac{1}{1+k^2} - \frac{1}{N_\epsilon \pi}$$

$$= 0.501\,87 - \frac{\epsilon}{\pi}.$$

The same analysis applies to a generic map when the zero approaches the boundary. Indeed the leading contribution is obtained by linearizing the map around the zero x_*. The integrand has the same structure as $A\epsilon/(B(x-x_*)^2 + \epsilon^2)$, where A and B are some constants, and the integration step must still be proportional to ϵ. Stenger's method is affected by a similar error. A more detailed analysis is given in Appendix B.

B. Number of zeroes

In order to evaluate the number of zeroes of the 2D map defined in (1), one has to introduce the extended function F_* defined by

$$F_* : \{x' = f_1(x,y), \quad y' = f_2(x,y), \quad z' = z \det J_F(x,y)\}, \tag{7}$$

where J_F denotes the Jacobian of (f_1, f_2). The function F_* has a Jacobian with non-negative determinant equal to $[\det J_F(x,y)]^2$ and the same zeroes as F on the x, y plane and consequently its TD $\mathcal{T}(F_*, \mathcal{D}_*)$, where $\mathcal{D}_* = \mathcal{D} \times [-\gamma, \gamma]$, $\gamma > 0$, gives the number of simple zeroes of the function F.

C. The Kronecker integral

The number of zeros can be evaluated by computing the TD of the 3D function F_* (7) via the Kronecker integral which in the 3D case becomes

$$\mathcal{T}(F_*, \mathcal{D}_*) = \frac{1}{2\pi} \int_{b(\mathcal{D})} (P_1 \, dx_1 + P_2 \, dx_2)$$
$$+ \frac{\gamma}{2\pi} \int\int_\mathcal{D} \frac{Q \, dx_1 \, dx_2}{(f_1^2 + f_2^2 + \gamma^2 J^2)^{3/2}}, \tag{8}$$

with

$$P_i = \frac{\left(f_1 \dfrac{\partial f_2}{\partial x_i} - f_2 \dfrac{\partial f_1}{\partial x_i}\right)\gamma J}{(f_1^2 + f_2^2)(f_1^2 + f_2^2 + \gamma^2 J^2)^{1/2}}, \quad i=1,2,$$

$$Q = \begin{vmatrix} f_1 & \dfrac{\partial f_1}{\partial x_1} & \dfrac{\partial f_1}{\partial x_2} \\[2mm] f_2 & \dfrac{\partial f_2}{\partial x_1} & \dfrac{\partial f_2}{\partial x_2} \\[2mm] J & \dfrac{\partial J}{\partial x_1} & \dfrac{\partial J}{\partial x_2} \end{vmatrix},$$

where $J = \det J_F$.
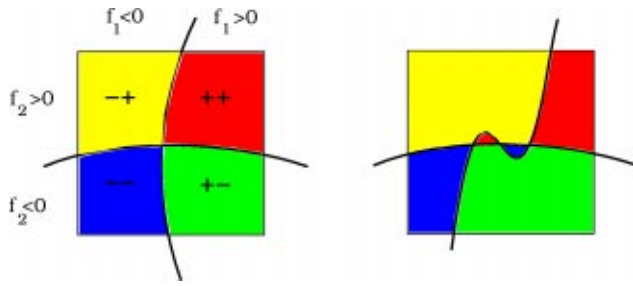
FIG. 1. (Color online) Sketch of the domains where f_1, f_2 have the indicated combination of signs.

D. The color map

One can use a *color map* to inspect the geometry of the 2D map M and to locate the zeroes. Choosing a regular lattice of $2^n \times 2^n$ cells of side $\epsilon = 2^{-n} \times 2L$ on the square $|x| \leq L$, $|y| \leq L$, we associate to each point a color chosen according to the signs of the functions f_1, f_2: red for $(+,+)$, green for $(+,-)$, yellow for $(-,+)$, blue for $(-,-)$ as shown in Fig. 1.

The plot of the *color map* on the lattice gives an immediate insight of where the zeroes are. We label by (i,j) the lattice points whose coordinates are $x = -L + i\epsilon$, $y = L - j\epsilon$, with $i,j = 0,...,2^n$, and by $c_m(i,j)$ the box of side $m\epsilon$ whose vertices are $A = (i,j)$, $B = (i+m,j)$, $C = (i,j+m)$, $D = (i+m,j+m)$. A simple algorithm allows to detect the boxes $c_1(i,j)$ whose vertices have four distinct colors. These boxes are candidates to have a zero in their interior. To detect the zeroes of the map up to an accuracy ϵ one should test its signs at the interior points of each box $c_1(i,j)$, since the presence of different signs at the vertices of a box is neither necessary nor sufficient for the presence of a zero in its interior. Considering instead the boxes c_m, with $2 \leq m \leq n$, we check again the presence of four distinct colors at all the lattice points within these boxes. For fixed m we scan all the boxes $c_m(i,j)$ with $i,j = 0,...,2^n - m + 1$ selecting those which satisfy the above four-colors criterion. The boxes $c_m(i,j)$ overlap and the accuracy in the localization of zeroes is the box size $m\epsilon$. As a consequence among all the boxes which satisfy the four-colors criterion we select the box $c_m(i,j)$ discarding all the overlapping boxes $c_m(i',j')$, where $\max(|i'-i|,|j'-j|) \leq m-1$. By increasing m from 1 to n the number of four colors nonoverlapping boxes $c_m(i,j)$ reaches a constant value provided that the distance of zeroes is bigger than $n\epsilon$. Of course in the ideal limit $n \to \infty$ the exact result is recovered.

III. FIXED POINTS

Given a map M the periodic points of period p are fixed points of $M^{\circ p}$ and the zeroes of the map

$$F = M^{\circ p} - I.$$

We have considered the HM, BM, and SM maps which are, respectively, unbounded on $\mathbb{R}^2$, bounded on $\mathbb{R}^2$ and defined as an application of the torus into itself. Their explicit expressions are

$$HM: \begin{pmatrix} x' \\ y' \end{pmatrix} = R(\omega) \begin{pmatrix} x \\ y + x^2 \end{pmatrix},$$

$$BM: \begin{pmatrix} x' \\ y' \end{pmatrix} = R(\omega) \begin{pmatrix} x \\ y + 1 - e^{-x^2} \end{pmatrix},$$

where $R(\omega)$ is an orthogonal 2×2 matrix representing a clockwise rotation by angle $2\pi\omega$. The true beam–beam map has $(1 - e^{-x^2})/x$ but we consider this modified version since it has very similar properties and becomes the Hénon map for $x \to 0$. SM is defined on the torus $[-\frac{1}{2},\frac{1}{2}] \times [-\frac{1}{2},\frac{1}{2}]$ according to

$$SM: \begin{cases} x' = x + y - \dfrac{\kappa}{2\pi} \sin 2\pi x \bmod \left(1, \dfrac{1}{2}\right), \\ y' = y - \dfrac{\kappa}{2\pi} \sin 2\pi x \bmod \left(1, \dfrac{1}{2}\right), \end{cases}$$

$$x \bmod(1,\tfrac{1}{2}) \equiv x \bmod 1 + \begin{cases} -1 & \text{if } x \bmod 1 > \tfrac{1}{2}, \\ 1 & \text{if } x \bmod 1 < -\tfrac{1}{2}. \end{cases} \tag{9}$$

For the beam–beam map with $\omega = 0.21$ we have computed the *color map* for fixed points of period $p = 5$ (see Fig. 2).

We have searched for the fixed points in boxes of increasing size $m \geq 2$ and the results obtained for $m = 7$ are also shown in Fig. 2 (right) where the orbits of the map are shown for comparison. The results for the total number $\mathcal{N}_5$ of fixed points of period 5 using the algorithm described in the preceding section are the following:

m	2	3	4	5	6	7	8	9	10	
$\mathcal{N}_5$	12	24	29	30	30	30	31	31	31	exact=31

There is no evident relation between the size of the islands and the angle formed by the boundaries of the intersecting regions where (f_1,f_2) have given signs. When this angle is very small as for the top left island of Fig. 2, the size m of the box has to be increased considerably in order to detect the fixed point. In particular, for $m \leq 7$ one elliptic fixed point of the outer chain is not detected (right panel of Fig. 2).

For completeness we report in Fig. 3 the same *color-map* analysis for the HM with the same value of ω; the pattern is simpler with respect to BM, allowing an easy evaluation of the period 5 fixed points.

We have also examined the behavior of the standard map for a value $\kappa/2\pi = 0.9$ at which a very rich structure is present because we are approaching the global chaotic transition occurring when the last invariant curve breaks at $\kappa_c/2\pi \approx 0.97$.[6] The *color map* is given in Fig. 4 for the third iterate and the phase plot of the orbits is given for comparison. In this case the *color map* gives the fixed points of order 3 correctly and also some other four-color crossing which does not correspond to fixed points of the same period. Indeed they are located exactly on the third iterate of a discontinuity curve where the two components of the map change sign due to the modulus operation. The discontinuity curves and their iterated images cause problems in the application of methods for computing the TD (see Appendix C). When the map is
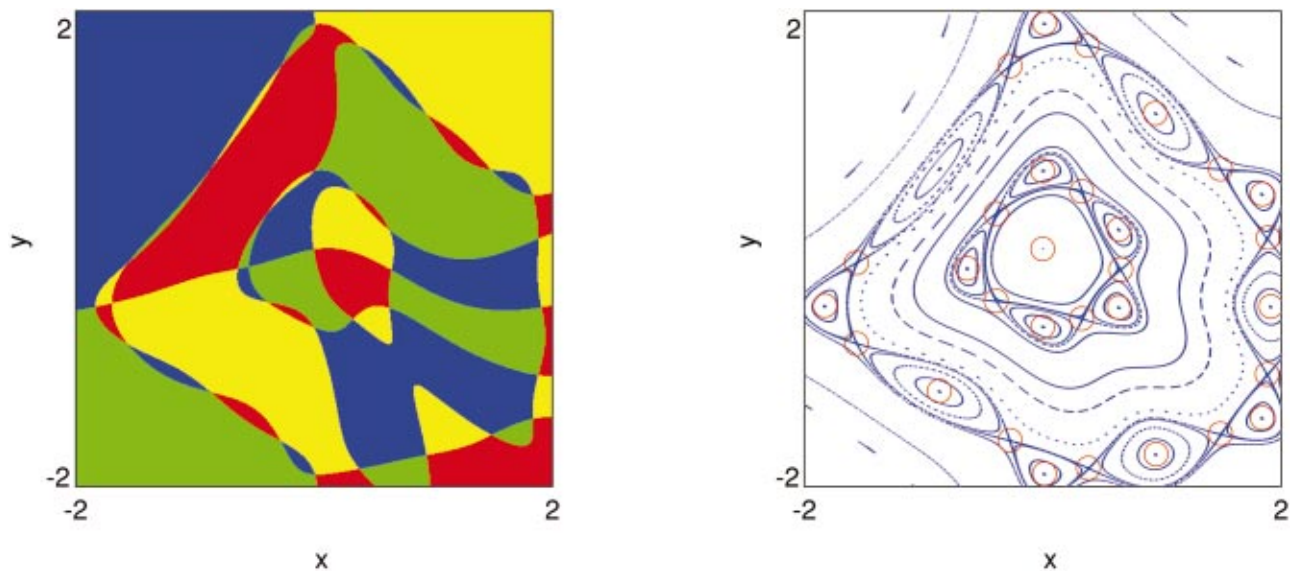
FIG. 2. (Color) Beam–beam map for $\omega=0.21$: *color map*, for $p=5$ iterations of the map, computed on a square lattice of $2^n \times 2^n$ points with $n=9$ (left); phase plot of the map (right): the red circles denote the position of the fixed points found with initial guesses taken in boxes of size $m\epsilon$ with $\epsilon=2^{-n}$ and $m=7$.

iterated these discontinuity curves are also iterated and the direct application of the TD method gives a wrong result. The number $\mathcal{N}_p$ of fixed points of period p has also been evaluated by computing the TD of the 3D function F_* (7) via the Kronecker integral (8). This integral has been evaluated numerically and gives accurate results if the map is bounded and continuous. The beam–beam map has this property for every compact domain $\mathcal{D} \subset \mathbb{R}^2$. The standard map has discontinuity curves, the Hénon map is unbounded. Due to this last property the TD cannot be computed with the same accuracy as the BM and for this reason we shall no longer analyze the HM in the rest of the paper, although the characteristic bisection method works fine for the HM too. For the beam–beam map considered in Fig. 2 where $\omega=0.21$ and $L=2$ the exact number of period five fixed points is 31.

This number is obtained within 1% error using a repeated four points Gauss integration with just 100×100 points. When the linear frequency is $\omega=0.14$ many periodic orbits of period 8, 9, 15 are present, as can be seen in Fig. 5. Choosing $p=8$ and $L=5$ requires a rather small number of grid points on the boundary ($N=2100$) to reach the correct value $\mathcal{N}_8=33=1+2 \times 8+2 \times 8$ whereas the correct value $\mathcal{N}_9=37=1+2 \times 9+2 \times 9$ for $p=9$ is reached much sooner. In both cases there are two chains of fixed points, but for $p=9$ they both have significantly big stability basins, while for $p=8$ one of them is very thin and embedded in a region of the phase space almost entirely filled by "invariant curves." For higher values of p the computation becomes extremely time consuming.
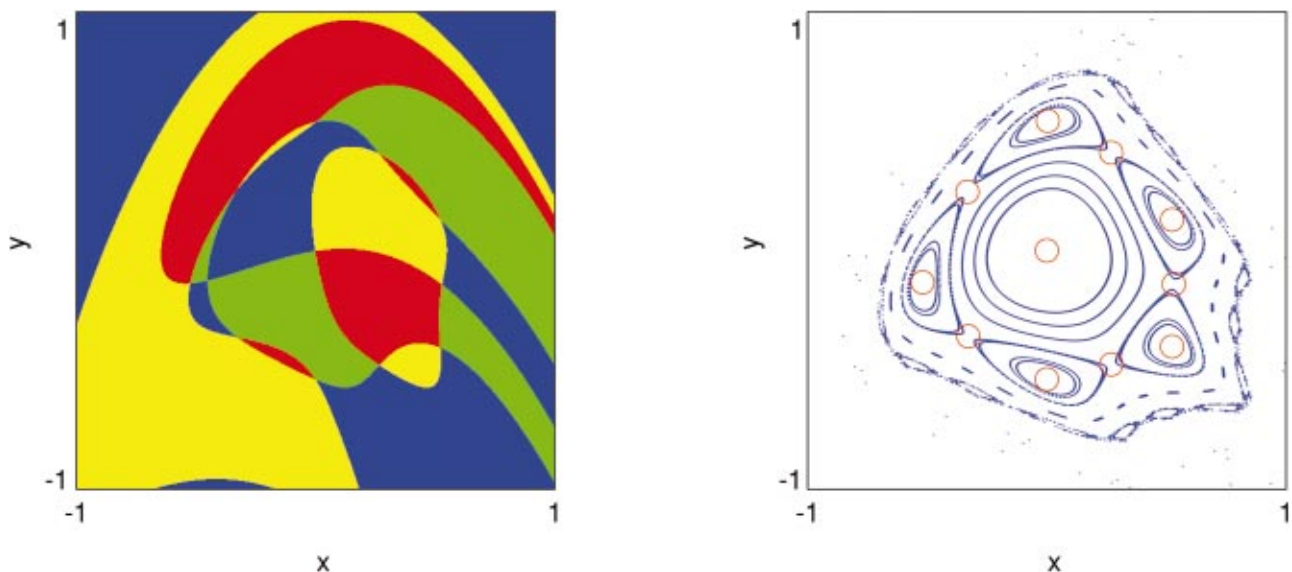
FIG. 3. (Color) Hénon map for $\omega=0.21$: *color map*, for $p=5$ iterations of the map, computed on a square lattice of $2^n \times 2^n$ points with $n=9$ (left); phase plot of the map (right): the red circles denote the position of the fixed points found with initial guesses taken in boxes of size $m\epsilon$ with $\epsilon=2^{-n}$ and $m=7$.
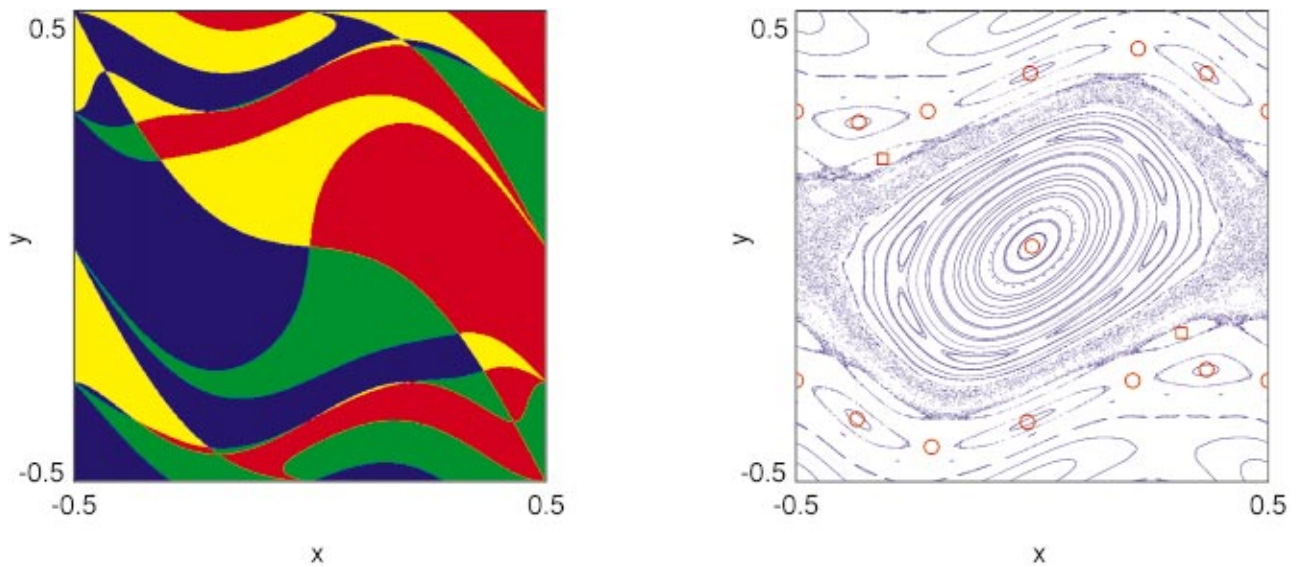
FIG. 4. (Color) Standard map with $\kappa/2\pi = 0.9$: *color map*, for $p = 3$ iterations of the map, computed on a square lattice of $2^n \times 2^n$ points with $n = 9$ (left); phase plot of the map (right); the red circles denote the position of the fixed points found with initial guesses taken in boxes of size $m\epsilon$ with $\epsilon = 2^{-n}$ and $m = 7$; the red squares mark the position of two evident four-color crossings in the *color map* which do not correspond to period 3 fixed points but rather to period 4 fixed points lying just on the third iterate of a discontinuity curve.

The characteristic bisection method

The TD method cannot be used directly to locate the fixed points of a map. When the boundedness and continuity conditions occur the Kronecker integral allows to compute the number of fixed points in a given domain provided that the integration step is small enough (smaller than the distance of fixed points from the boundary and from each other); the required evaluation of the derivatives of $M^{\circ p}$ can be cumbersome and numerically expensive for large p. The *color-map* method is a simple algorithm to have a first guess, which can be refined by using the characteristic bisection method.

Another approach consists in applying the characteristic bisection method to all the cells $c_1(i,j)$ of a lattice, where the topological degree is $\mathcal{T} = \pm 1$. Since the computational cost of an accurate evaluation of $\mathcal{T}$ is high, it is more convenient to check whether or not the pth iterated of the cell's center through the map comes back inside the cell and only when this happens one tries to apply the characteristic bisection method to these "candidate" cells. To speed up considerably one can restrict further the characteristic bisection method only to cells which are characteristic polyhedra (the vertices have four distinct combinations of signs or colors).

This procedure misses some fixed points and their num-
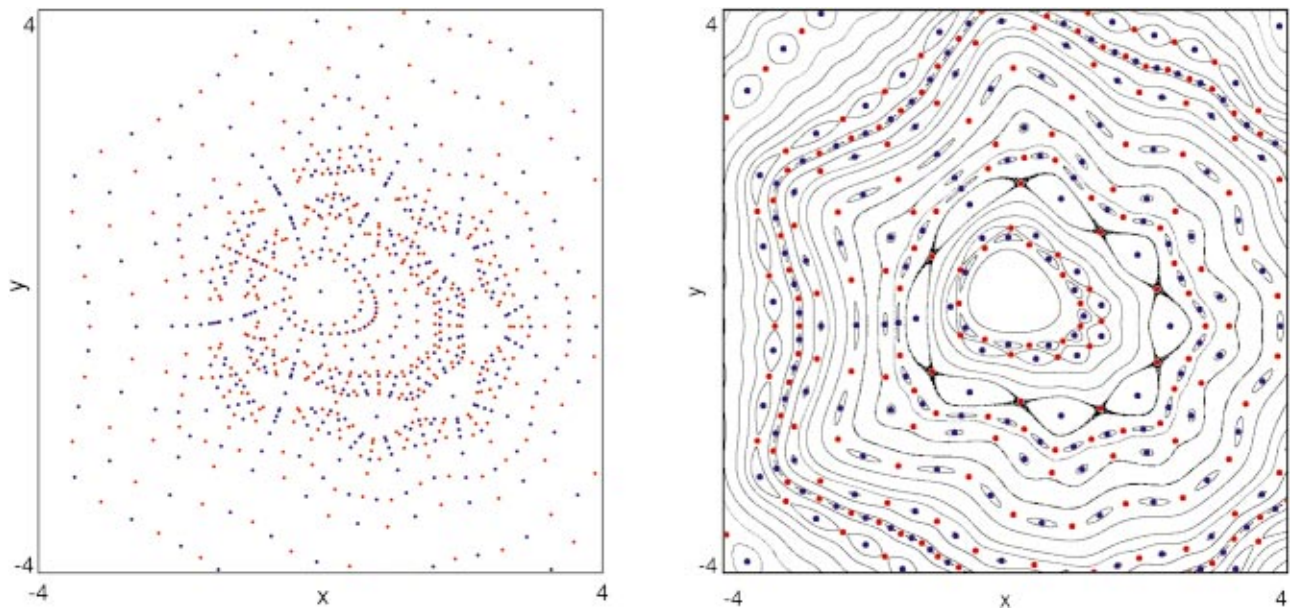
FIG. 5. (Color) Fixed points up to order $p = 40$ for the BM map with linear frequency $\omega = 0.14$ (left) computed on a lattice with 1000×1000 grid points. The elliptic fixed points are blue and the hyperbolic points are red. Phase plot for the same map (right), with fixed points determined through a visual initial guess.
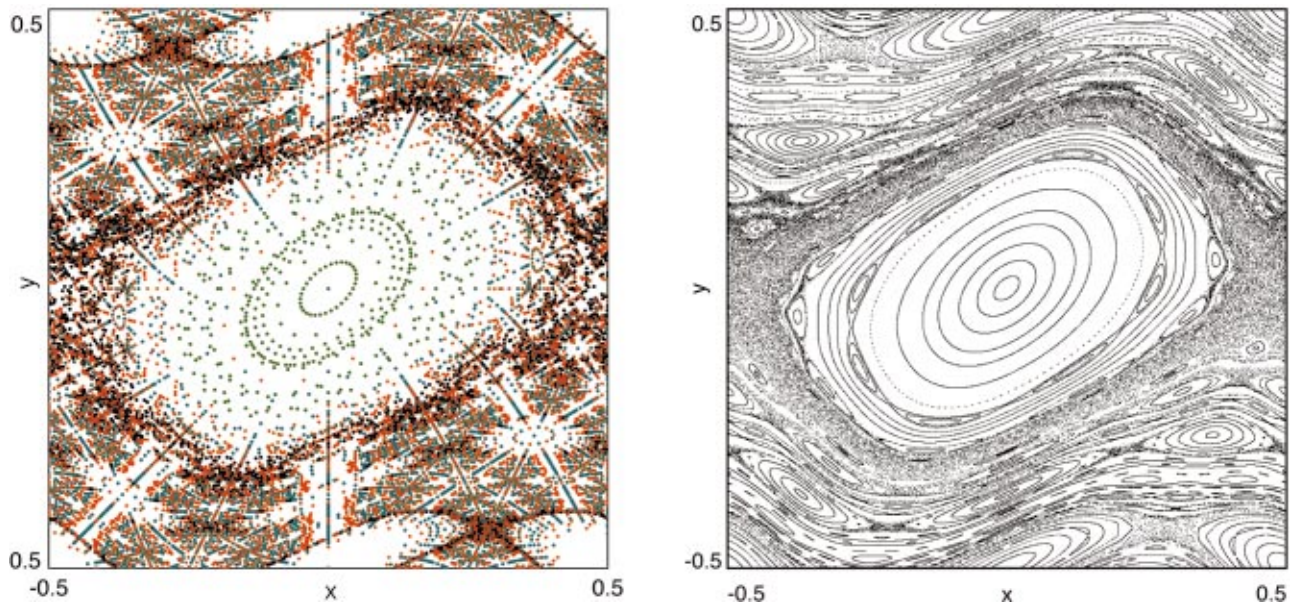
FIG. 6. (Color) Fixed points up to order $p = 40$ for the standard map with $\kappa/2\pi = 0.9$ (left) computed on a lattice with 2000×2000 grid points. The elliptic fixed points are blue, the parabolic points green, the hyperbolic points are red, the hyperbolic points with reflection dark. Phase plot for the same map (right) with orbits started at initial points taken from the left picture.

ber depends on the angle α between the tangents to the lines $(M^{\circ p} - I)_x = 0$, $(M^{\circ p} - I)_y = 0$ at the intersection point. A good strategy to recover these fixed points too would be looking for a characteristic polyhedron which not necessarily coincides with any of the lattice cells: this could be achieved by evaluating the signs of $(M^{\circ p} - I)$ over the perimetric vertices of a larger ''macro-cell'' built up with several adjacent elementary cells of our lattice surrounding the one which was ''candidate'' for a fixed point in its interior. When the size of this ''macro-cell'' is large enough (and of course not greater than a preset maximum size) it is likely that all four combinations of signs can be found on the perimetric vertices, a necessary condition to construct a characteristic polyhedron.

If the cell side is $\epsilon = 2^{-n} \times 2L$ and we allow for k bisections the overall computational complexity is $p(p+1)k2^{2n}$ evaluations of the map to obtain the fixed points up to period p with an accuracy of $\epsilon 2^{-k} = L2^{-n-k+1}$. Typically choosing $k = 40$ when $L = 1$ the machine accuracy is reached. In this case for a typical grid corresponding to screen resolution ($n = 10$) the number of functions evaluation is $\sim 10^{10}$ to compute the fixed points up to period $p = 20$. We have applied this procedure to locate the fixed points in the beam–beam map for $\omega = 0.14$ in the square $[-L,L]^2$ with $L = 5$. The search for fixed points up to order $q = 40$ with a grid $2^n \times 2^n$ with $n = 10$ was successful as confirmed by a comparison with a manually initialized search driven by an interactive phase space portrait drawing. In Fig. 5 we show this comparison. The nature of the fixed points has been examined and to the elliptic and hyperbolic points a different color (blue and red, respectively) has been assigned. The overall picture shows very neatly the invariant curves near to central elliptic fixed point and the doublets of elliptic and hyperbolic points corresponding to the resonances (islands).

The same picture has been obtained for the standard map

(see Fig. 6), where one finds also parabolic (with $||\mathrm{Tr} J_F| - 2| < 10^{-6}$) and hyperbolic with reflection fixed points (marked in green and dark, respectively): in this case the problem may occur only at the discontinuity curves which produce four-color crossings in the *color map* which do not correspond to fixed points of the same period as the one used to draw the *color map* itself. There are also points on the torus ''boundary'' ($x = \pm\frac{1}{2}$ or $y = \pm\frac{1}{2}$) where more than four regions of different colors meet. However, all these ''discontinuity effects'' turn out to correspond to fixed points of some period so that they are correctly found through the characteristic bisection method which looks for fixed points of periods ''up to'' a preset maximum value. The characteristic bisection method, in turn, is not affected by the presence of the discontinuity curves images (which in any case are of measure 2^{-n} with respect to 1). We have chosen a value of the parameter $\kappa/2\pi = 0.9$ not far from the critical one, where the last KAM curve is broken. The picture of the fixed points up to order 40 reflects the complexity of the dynamics in this transition region. The chaotic area is filled with hyperbolic fixed points, most of which are hyperbolic with reflection. The configuration of the fixed points on the plane seen in the left panel of Fig. 6, is similar to the distribution of periodic orbits of 2D Hamiltonian flows.[31]

IV. SUMMARY AND CONCLUSIONS

We have studied the applicability of various numerical methods, based on the topological degree theory, for locating high period periodic orbits of 2D area preserving mappings. In particular we have used the Kronecker integral and applied Stenger's method for finding the TD in a bounded region of the phase space. If the TD has a nonzero value we know that there exists at least one periodic orbit in the corresponding region. The computation of the TD for an appropriate set of equations allows us to also find the exact num-

ber of periodic orbits. We also applied the characteristic bisection method on a grid in the phase space for locating the various fixed points. The main advantage of all these methods is that they are not affected by accuracy problems in computing the exact values of the various functions used, since the only computable information needed is the algebraic signs of these values.

We have applied the above-mentioned methods to 2D symplectic mappings defined on $\mathbb{R}^2$ and on the torus $\mathbb{T}^2$. The methods for computing the TD are limited to regions without discontinuity curves, so they cannot be used for maps on the torus, since upon iterating the map the discontinuity curves form a web, whose limit is a dense subset. On the other hand, the characteristic bisection method proved to be very efficient for all different types of mappings, since it could provide, in reasonably short computational times, a number of fixed points of period as large as 40 which allows a satisfactory description of the underlying dynamics, as it has been shown in recent works.[32,33] The good performance of the bisection method for the maps on the torus can be explained by the structure of the discontinuity curves. For a periodic orbit of order p the discontinuity curves to be considered are $\mathcal{D}_p = M^{-\circ p}(\mathcal{D}_0)$ where $\mathcal{D}_0$ is the set of discontinuity curves, which in the case of SM are the lines $x = -\frac{1}{2}$ and $y = -\frac{1}{2}$. The periodic points of period p are found by applying the characteristic bisection method to the map $M^{\circ p}$ on squares of side $\epsilon = 2^{-n}L$, which are characteristic polyhedra. As a consequence the characteristic bisection method is not affected by the presence of the discontinuity curves as far as the distance of the periodic points from the set $\mathcal{D}_p$ is larger than ϵ.

ACKNOWLEDGMENTS

APPENDIX A: CHARACTERISTIC BISECTION

Many problems in different areas of science and technology can be reduced to a study of a set of solutions of a system of nonlinear equations of the form:

$$\mathbf{F}(\mathbf{X}) = \mathbf{0}, \tag{A1}$$

in an appropriate space. Topological degree theory has been developed as means of examining this solution set and obtaining information on the existence of solutions, their number and their nature.[8–11,34] This theory is widely used in the study of nonlinear transcendental or differential (ordinary and partial) equations.[7,14,15,19,25–27,35] It is useful, for example, in bifurcation theory and for providing information about the existence and stability of periodic solutions of ordinary differential equations as well as the existence of solutions of certain partial differential equations. Several of these applications involve the use of various fixed point theorems which can be provided by means of topological degree.[16,36]

Next, we will briefly discuss the characteristic bisection method based on the characteristic polyhedron concept for the computation of periodic orbits. The problem of finding periodic orbits of period p of dynamical systems in $\mathbb{R}^{n+1}$ amounts to finding the fixed points of the Poincaré map $M(\mathbf{X})$ in $\mathbb{R}^n$ with $\mathbf{X} \in \mathbb{R}^n$, by solving the equation $M^{\circ p}(\mathbf{X}^*) = \mathbf{X}^*$.

1. Characteristic polyhedra

The search of periodic points of a mapping is equivalent to solving the system of Eq. (A1) with $\mathbf{F} = (f_1, f_2, \ldots, f_n) = M^{\circ p} - I_n$, where I_n is the identity and $\mathbf{0} = (0,0,\ldots,0)$ is the origin of $\mathbb{R}^n$. It is well known that if we have a function $\mathbf{F}$, which is continuous in an open and bounded domain $\mathcal{D}$ and the topological degree of $\mathbf{F}$ at $\mathbf{0}$ relative to $\mathcal{D}$ is not equal to zero, then there is at least one solution of system (A1) within $\mathcal{D}$. This criterion can be used, in combination with the construction of a suitable n polyhedron, called the characteristic polyhedron, for the calculation of a solution contained in this region. This can be done as follows. Let $\mathcal{M}_n$ be the $2^n \times n$ matrix whose rows are formed by all possible combinations of -1 and 1. Consider now an oriented n polyhedron Π^n, with vertices $\mathbf{V}_k$, $k = 1, \ldots, 2^n$. If the $2^n \times n$ *matrix of signs associated with* $\mathbf{F}$ *and* Π^n, $\mathcal{S}(\mathbf{F}; \Pi^n)$, whose entries are the vectors

$$\operatorname{sign} \mathbf{F}(\mathbf{V}_k) = (\operatorname{sign} f_1(\mathbf{V}_k), \operatorname{sign} f_2(\mathbf{V}_k), \ldots, \operatorname{sign} f_n(\mathbf{V}_k)),$$

is identical to $\mathcal{M}_n$, possibly after some permutations of these rows, then Π^n is called the *characteristic polyhedron relative to* $\mathbf{F}$. Furthermore, if $\mathbf{F}$ is continuous, then, under some suitable assumptions on the boundary of Π^n,

$$\deg[\mathbf{F}, \Pi^n, \mathbf{0}] = \sum_{\mathbf{X} \in \mathbf{F}^{-1}(\mathbf{0}) \cap \mathring{\Pi}^n} \operatorname{sign} \det J_{\mathbf{F}}(\mathbf{X}) = \pm 1 \neq 0,$$

(where $\deg[\mathbf{F}, \Pi^n, \mathbf{0}]$ denotes the topological degree of $\mathbf{F}$ at $\mathbf{0}$ relative to Π^n, $\mathring{\Pi}^n$ determines the interior of Π^n and $\det J_{\mathbf{F}}(\mathbf{X})$ denotes the determinant of the Jacobian matrix at $\mathbf{X}$), which implies the existence of a periodic orbit inside Π^n.

Next, we describe the *characteristic bisection method*. This method simply amounts to constructing another refined characteristic polyhedron, by bisecting a known one, say Π^n, in order to determine the solution with the desired accuracy. We compute the midpoint $\mathbf{M}$ of an 1-simplex, e.g., $\langle \mathbf{V}_i, \mathbf{V}_j \rangle$, which determines a one-dimensional edge of Π^n. The endpoints of this one-dimensional line segment are vertices of Π^n, for which the corresponding coordinates of the vectors, $\operatorname{sign} \mathbf{F}(\mathbf{V}_i)$ and $\operatorname{sign} \mathbf{F}(\mathbf{V}_j)$ differ from each other only in one entry. We call this 1-simplex proper 1-simplex. To obtain another characteristic polyhedron Π^n_* we compare the sign of $\mathbf{F}(\mathbf{M})$ with that of $\mathbf{F}(\mathbf{V}_i)$ and $\mathbf{F}(\mathbf{V}_j)$ and substitute $\mathbf{M}$ for that vertex for which the signs are identical. Subsequently, we reapply the aforementioned technique to a different edge (for details we refer to Refs. 7, 17, 18). In particular, let $\langle \mathbf{V}_i, \mathbf{V}_j \rangle$ be a proper 1-simplex of Π^n and let $\mathbf{B} = (\mathbf{V}_i + \mathbf{V}_j)/2$ be its midpoint. We then distinguish the following three cases:

(1) If the vectors $\operatorname{sign} \mathbf{F}(\mathbf{B})$ and $\operatorname{sign} \mathbf{F}(\mathbf{V}_i)$ are identical $\mathbf{B}$ replaces $\mathbf{V}_i$ and the process continues with the next proper 1-simplex.
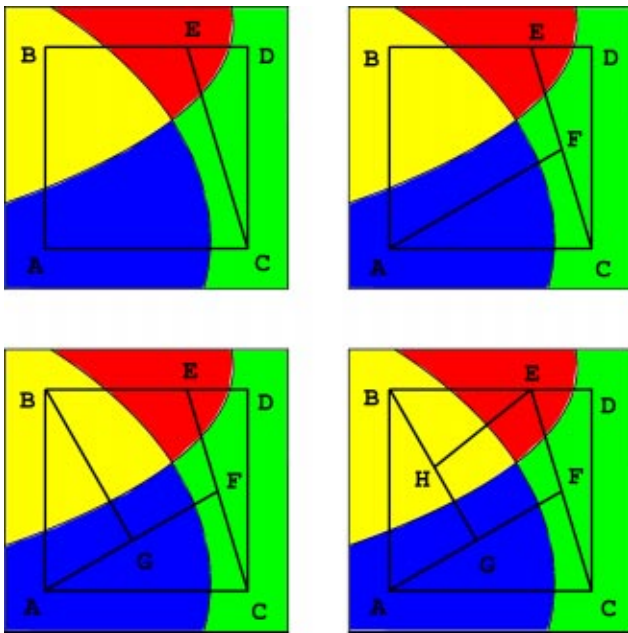
FIG. 7. (Color online) Application of the characteristic bisection method. The different gray tones correspond to the sign combination $(+,+)$, $(+,-)$, $(-,+)$, and $(-,-)$. $ABEC$, $BEFA$, $BEFG$, and $HEFG$ are characteristic polyhedra constructed by the successive application of the characteristic bisection method.

(2) If the vectors sign $\mathbf{F}(\mathbf{B})$ and sign $\mathbf{F}(\mathbf{V}_j)$ are identical then $\mathbf{B}$ replaces $\mathbf{V}_j$ and the process continues with the next proper 1-simplex.

(3) Otherwise the process continues with the next proper 1-simplex.

Consider the characteristic n polyhedron, Π^n, whose longest edge length is $\Delta(\Pi^n)$. The minimum number ζ of bisections of the edges of Π^n required to obtain a characteristic polyhedron Π^n_* whose longest edge length satisfies $\Delta(\Pi^n_*) \leq \epsilon$, for some accuracy $\epsilon \in (0,1)$, is given by $\zeta = \lceil \log_2(\Delta(\Pi^n)\epsilon^{-1}) \rceil$, where $\lceil \rceil$ denotes the largest integer which is smaller than the quoted number. Notice that ζ is independent of the dimension n, implying that the bisection algorithm performs the same number of iterations as the bisection in one dimension, which is optimal and asymptotically possesses the best rate of convergence.[37] The characteristic bisection method is efficient for low dimensions, because the computational effort for applying it grows as a power of the dimensionality n, since the starting box as well as the characteristic polyhedron have 2^n vertices.

2. Mappings of $\mathbb{R}^2$

To clarify the characteristic polyhedron concept we consider a function $\mathbf{F} = (f_1, f_2)$. Each function f_i, $i = 1,2$, separates the space into a number of different regions, according to its sign, for some regions $f_i < 0$ and for the rest $f_i > 0$, $i = 1,2$. Thus, in Fig. 7 we distinguish between the regions marked with distinct colors: $(+,+)$ red region where $f_1 > 0$ and $f_2 > 0$, $(+,-)$ green region where $f_1 > 0$ and $f_2 < 0$, $(-,+)$ yellow region where $f_1 < 0$ and $f_2 > 0$ and $(-,-)$ blue region where $f_1 < 0$ and $f_2 < 0$. Picking a point, close to the

solution, from each of the four regions we construct a characteristic polyhedron. In this figure we can distinguish a characteristic and a noncharacteristic polyhedron Π^2. For a polyhedron Π^2 to be characteristic all the above combinations of signs must appear at its vertices. Based on this criterion, polyhedron $ABDC$ is not a characteristic polyhedron, whereas $ABEC$ is. To fully comprehend the characteristic bisection method we illustrate in Fig. 7 its repetitive operation on a characteristic polyhedron Π^2. Starting from the edge CE we find its midpoint F and then calculate its vector of signs, which is $(+1,-1)$. Thus, vertex F replaces C, which has the same vector of signs, and the new refined polyhedron $BEFA$ is also characteristic. Applying the same procedure, we further refine the polyhedron by considering the midpoint G of AF and checking the vector of signs at this point. In this case, its vector of signs is $(-1,-1)$, so that vertex A can be replaced by vertex G. Finally we consider the midpoint H of BG. Since the vector of signs is $(-,+)$ we replace B with H. The new refined polyhedron $HEFG$ is also characteristic. This procedure continues up to the point that the midpoint of the longest diagonal of the refined polyhedron approximates the root within a predetermined accuracy. The characteristic bisection method is very useful in cases where the period of the periodic orbit is very high and especially when the orbit is unstable, since the method always converges within the initially specified region. A further advantage of the characteristic bisection method is the simplicity of location of all periodic orbits of a given period. From a pictorial point of view this is achieved by assigning a color to each region as in Fig. 7.

It is evident that in a neighborhood of the zero of $\mathbf{F}(\mathbf{X})$ there are points having four distinct vectors of signs, namely four different colors. As a consequence the color plot is an effective way of understanding the structure of $\mathbf{F}(\mathbf{X})$ and detecting approximately the location of its zeroes. The characteristic bisection method then allows to detect them up to machine accuracy.

APPENDIX B: STENGER'S METHOD

In order to illustrate the basic features of Stenger's method for computing the TD we consider the simple function $F = (f_1, f_2)$ where $f_1(x,y) = y - (x^3/3) + x$ and $f_2(x,y) = y$. The lines $f_1 = 0$, $f_2 = 0$ are plotted in Fig. 8(a). The above system of equations has three roots. The determinant of the corresponding Jacobian matrix is positive for root $(0,0)$ and negative for roots $(-\sqrt{3},0)$ and $(\sqrt{3},0)$. In order to study the dependence of the procedure for finding the TD in a region $\mathcal{D}$, with respect to the distance of a root from the boundary of $\mathcal{D}$, we consider a rectangular area $[-a,2] \times [-2,2]$ with $a > \sqrt{3}$, shown in Fig. 8(a). Since this domain contains the three roots of the system, the value of TD is -1. We let $a = \sqrt{3} + \epsilon$ with $\epsilon > 0$ so that the boundary approaches the root $(-\sqrt{3},0)$ as $\epsilon \to 0$ as shown by the arrow in Fig. 8(a). We compute the TD for different values of ϵ with Stenger's method, by using the same number of points N on every side of the rectangle. The distance of the root from the boundary is ϵ and we denote with n_{gp} the smallest number of grid points needed to compute TD with certainty. The number of

(a) Plot of the curves $f_1 \equiv y - \frac{1}{3}x^3 + x = 0$ and $f_2 \equiv y = 0$.
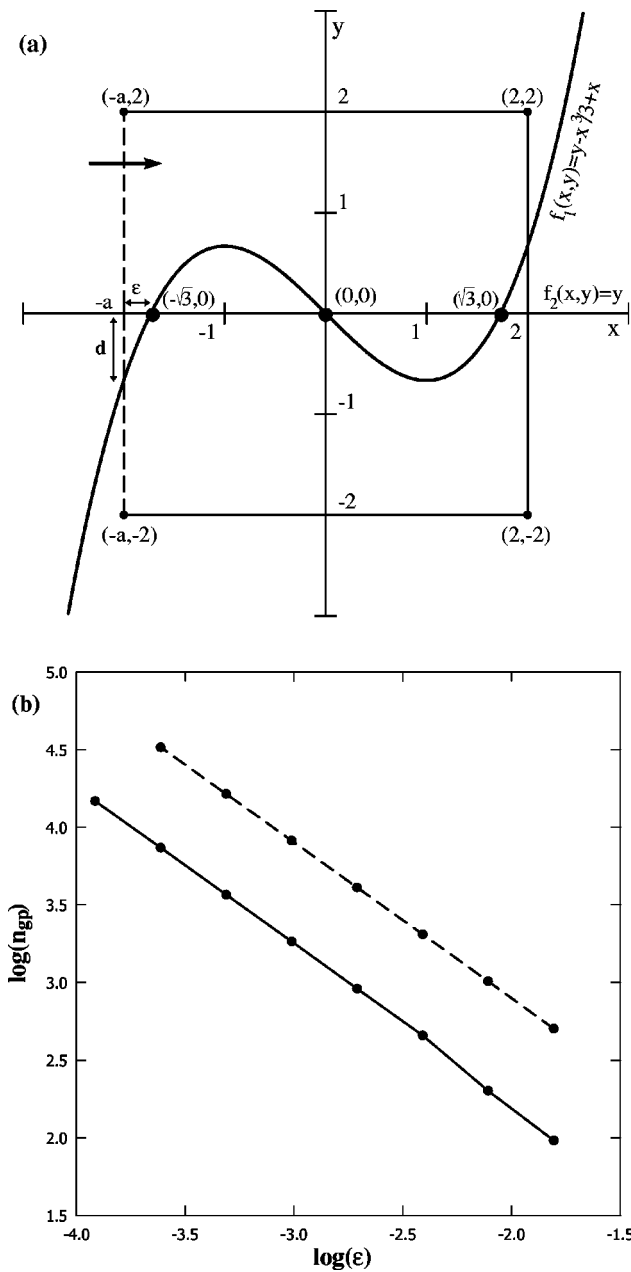
FIG. 8. (a) Plot of the curves $f_1 \equiv y - \frac{1}{3}x^3 + x = 0$ and $f_2 \equiv y = 0$. (b) Number of iteration points n_{gp} used to compute the correct value of the TD on a domain for the set of equation of panel (a) (dashed line) and the SM (continuous line), versus the distance ϵ of a root from the boundary of the domain.

FIG. 9. (Color online) Number of fixed points $\mathcal{N}_1$ evaluated for the standard map with $\kappa/2\pi = 0.9$ using the Kronecker integral, when the top side of the rectangular domain moves (a). The rectangle and the discontinuity curves are shown in (b). The discontinuity curves $x = -0.5$ and $y = -0.5$ are drawn as heavy gray lines, and the discontinuity curves that will be mapped on $x = -0.5$ and $y = -0.5$, after one iteration of the SM are shown.

total grid points used in the computation is $n_{gp} = 4N$. In Fig. 8(b) we plot in log–log scale, n_{gp} with respect to ϵ (dashed line). The slope of the curve is almost -1 so that $n_{\text{gp}} \propto \epsilon^{-1}$. The same result holds for any map when a root approaches the boundary. We have considered the standard map for $\kappa/2\pi = 0.9$ in the domain $[-0.25, 0.25] \times [-\epsilon, 0.25]$, with $\epsilon > 0$, free of discontinuity curves (see Appendix C), which contains the elliptic fixed point $(0,0)$. The value of TD is $+1$. We let $\epsilon \rightarrow 0$ and compute n_{gp} as a function of ϵ like in the previous case. As in the previous example we obtain the correct value of the TD when the grid step is of order ϵ as shown by the solid line in Fig. 8(b). These examples show how the computation of the TD based on Stenger's method is

affected by the presence of a root near the boundary. A similar behavior appears when we use the Kronecker integral for the computation of the total number of roots in a given domain $\mathcal{D}$.

APPENDIX C: DISCONTINUITY CURVES

For maps defined on the torus like the SM, the computation of the TD using Stenger's method or the Kronecker integral faces a problem due to the presence of discontinuity curves. Indeed the Kronecker integral is defined on a domain on the boundary of which the map is continuous. For the SM the discontinuity curves are the lines $x = -0.5$ and $y = -0.5$, plotted in blue and red color representatively Fig. 9(b). On the initial phase space there exist also the disconti-

nuity curves that will be mapped after one iteration to the lines $x = -0.5$ and $y = -0.5$. These curves are plotted in black and green color representatively in Fig. 9(b) and are produced by applying the inverse SM,

$$M^{-1} = \begin{cases} x = x' - y' \bmod(1,\tfrac{1}{2}), \\ y = y' + \dfrac{\kappa}{2\pi} \sin(2\pi x) \bmod\left(1,\dfrac{1}{2}\right), \end{cases}$$

to the discontinuity lines $x = -0.5$ and $y = -0.5$. So the discontinuity curves divide the initial phase space in five continuous regions.

In each region the computation of the TD can be performed accurately by Stenger's method or by the Kronecker integral evaluation. If however the boundary of the domain where these procedures are applied crosses a discontinuity curve the results we get are not correct. This behavior becomes evident in the case plotted in Fig. 9. We consider the set of rectangular areas $[-0.25, 0.15] \times [-0.25, y]$ with $0.25 \leqslant y < 0.5$, which contain the fixed point of period 1 (0,0). In these rectangles we compute the total number of roots $\mathcal{N}_1$ of period 1 (which should to be equal to 1), by evaluating the Kronecker integral (8). For our computation we use a 100×100 equally spaced grid. The upper side of the rectangle moves towards greater values of y in the direction indicated by the thick arrow in Fig. 9(b). The two points marked by arrows in Fig. 9(a), where $\mathcal{N}_1$ deviates from the correct value $\mathcal{N}_1 = 1$, correspond to $y \approx 0.358$ and $y \approx 0.466$, respectively, where the upper side of the rectangle crosses the two discontinuity curves [see Fig. 9(b)]. The behavior observed in Fig. 9(a) is due to the fact that the functions are not continuously differentiable in the given rectangles and does not depend on the inaccuracy of the integration (the results do not vary by refining the mesh up to $10^3 \times 10^3$). The computation of TD through Stenger's method faces the same problem. From this analysis it is evident that the TD cannot be evaluated for a map on the torus as the SM because by increasing the order p the discontinuity curves network becomes progressively more intricate.

[1] J. E. Howard and R. S. Mackay, "Linear stability of symplectic maps," J. Math. Phys. **28**, 1036–1051 (1987).

[2] Ch. Skokos, "On the stability of periodic orbits of high dimensional autonomous Hamiltonian systems," Physica D **159**, 155–179 (2001).

[3] J. E. Dennis and R. B. Schnabel, *Numerical Methods for Unconstrained Optimization and Nonlinear Equations* (SIAM, Philadelphia, 1996).

[4] J. M. Ortega and W. C. Rheinbolt, *Iterative Solution of Nonlinear Equations in Several Variables* (Academic, New York, 1970).

[5] M. Hénon, "Numerical study of quadratic area preserving mappings," Q. Appl. Math. **27**, 291 (1969).

[6] J. M. Greene, "A method for determining a stochastic transition," J. Math. Phys. **20**, 1183 (1979).

[7] M. N. Vrahatis, "An efficient method for locating and computing periodic orbits of nonlinear mappings," J. Comput. Phys. **119**, 105–119 (1995).

[8] N. G. Lloyd, *Degree Theory* (Cambridge University Press, Cambridge, 1978).

[9] L. Kronecker, *Werke* (Teubner, Leipzig, 1895), Vol. 1.

[10] E. Picard, "Sur le nombre des racines communes à plusieurs équations simultanées," J. Math. Pures Appl. **8**, 5–24 (1892).

[11] E. Picard, *Traité d' analyse*, 3rd ed. (Gauthier-Villars, Paris, 1922), Chap. 4.7.

[12] J. Hadamard, *Sur quelques propriétés de l'integrale de Kronecker* (Hermann, Paris, 1910).

[13] B. J. Hoenders and C. H. Slump, "On the calculation of the exact number of zeros of a set of equations," Computer **30**, 137–147 (1983).

[14] D. J. Kavvadias and M. N. Vrahatis, "Locating and computing all the simple roots and extrema of a function," SIAM J. Sci. Comput. (USA) **17**, 1232–1248 (1996).

[15] D. J. Kavvadias, F. S. Makri, and M. N. Vrahatis, "Locating and computing arbitrarily distributed zeros," SIAM J. Sci. Comput. (USA) **21**, 954–969 (1999).

[16] B. Mourrain, M. N. Vrahatis, and J. C. Yakoubsohn, "On the complexity of isolating real roots and computing with certainty the topological degree," J. Complexity **18**, 612–640 (2002).

[17] M. N. Vrahatis, "Solving systems of nonlinear equations using the nonzero value of the topological degree," ACM Trans. Math. Softw. **14**, 312–329 (1988).

[18] M. N. Vrahatis, "CHABIS: A mathematical software package for locating and evaluating roots of systems of nonlinear equations," ACM Trans. Math. Softw. **14**, 330–336 (1988).

[19] M. N. Vrahatis, T. Bountis, and M. Kollmann, "Periodic orbits and invariant surfaces of 4D nonlinear mappings," Int. J. Bifurcation Chaos Appl. Sci. Eng. **8**, 1425–1437 (1996).

[20] M. N. Vrahatis, H. Isliker, and T. C. Bountis, "Structure and breakdown of invariant tori in a 4-D mapping model of accelerator dynamics," Int. J. Bifurcation Chaos Appl. Sci. Eng. **7**, 2707–2722 (1997).

[21] G. Servizi, D. Bortolotti, E. Todesco, M. Giovannozzi, and M. N. Vrahatis, "GIOTTO: An interactive computer program for the analysis of 2D area preserving maps," Int. J. Mod. Phys. C **6**, 651–661 (1995).

[22] C. Polymilis, G. Servizi, and Ch. Skokos, "A quantitative bifurcation analysis of 2D like Henon maps," Celest. Mech. Dyn. Astron. **66**, 365–385 (1997).

[23] C. Polymilis, Ch. Skokos, G. Kollias, G. Servizi, and G. Turchetti, "Bifurcations of beam–beam like maps," J. Phys. A **33**, 1055–1064 (2000).

[24] F. Rannou, "Numerical study of discrete area preserving mappings," Astron. Astrophys. **31**, 289 (1974).

[25] V. S. Kalantonis, E. A. Perdios, A. E. Perdiou, and M. N. Vrahatis, "Computing with certainty individual members of families of periodic orbits of a given period," Celest. Mech. Dyn. Astron. **80**, 81 (2001).

[26] M. N. Vrahatis, A. E. Perdiou, V. S. Kalantonis, E. A. Perdios, K. Papadakis, R. Prosnliti, and S. C. Farantos, "Application of the characteristic bisection method for locating and computing periodic orbits in molecular systems," Comput. Phys. Commun. **138**, 53 (2001).

[27] E. A. Perdios, V. S. Kalantonis, and M. N. Vrahatis, "Efficient method for computing with certainty periodic orbits on a surface of section," Celest. Mech. Dyn. Astron. **84**, 231 (2002).

[28] F. Stenger, "Computing the topological degree of a mapping in $\mathbb{R}^n$," Numer. Math. **25**, 23–38 (1978).

[29] A. Bazzani, G. Servizi, E. Todesco, and G. Turchetti, "Normal form approach to the theory of nonlinear betatronic motion," CERN Yellow Report 94/02, 1994.

[30] B. V. Chirikov, "Universal instability of many-dimensional oscillator systems," Phys. Rep. **52**, 263–379 (1979).

[31] G. Contopoulos, E. Grousouzakou, and C. Polymilis, "Distribution of periodic orbits and the homoclinic tangle," Celest. Mech. Dyn. Astron. **64**, 363–381 (1996).

[32] C. P. Dettmann and G. P. Morriss, "Stability ordering of cycle expansions," Phys. Rev. Lett. **78**, 4201 (1997).

[33] C. P. Dettmann and P. Dahlqvist, "Computing the diffusion coefficient for intermittent maps: Resummation of stability ordered cycle expansions," Phys. Rev. E **57**, 5303 (1998).

[34] J. Cronin, *Fixed Points and Topological Degree in Nonlinear Analysis*, Mathematical Surveys No. 11 (American Mathematical Society, Providence, RI, 1964).

[35] L. Drossos, O. Ragos, M. N. Vrahatis, and T. C. Bountis, "Method for computing long periodic orbits of dynamical systems," Phys. Rev. E **53**, 1206–1211 (1996).

[36] M. N. Vrahatis, "A short proof and a generalization of Miranda's existence theorem," Proc. Am. Math. Soc. **107**, 701–703 (1989).

[37] K. Sikorski, "Bisection is optimal," Numer. Math. **40**, 111 (1982).